Advanced Powder Technology 33 (2022) 103440

Contents lists available at ScienceDirect

Advanced Powder Technology

journal homepage: www.elsevier.com/locate/apt

Understanding the formation of ultrafine maltodextrin particles under simultaneous convective drying and antisolvent vapour precipitation

Kian Siang Lim [a], Nan Fu [d], Jie Xiao [d], Xiao Dong Chen [d], Cordelia Selomulya [a,c], Meng Wai Woo [a,b,*]

[a] Department of Chemical and Biological Engineering, Monash University, Clayton Campus, VIC 3800, Australia
[b] Department of Chemical and Materials Engineering, University of Auckland, Auckland 1023, New Zealand
[c] School of Chemical Engineering, UNSW Sydney, NSW 2052, Australia
[d] School of Chemical and Environmental Engineering, College of Chemistry, Chemical Engineering and Materials Science, Soochow University, Suzhou, Jiangsu 215123, China

ARTICLE INFO

Article history:
Received 11 September 2021
Received in revised form 13 December 2021
Accepted 17 January 2022

Keywords:
Ethanol-vapour-induced precipitation
Particle morphology
Mass profiles
Internal compositions
Mass ratio

ABSTRACT

Research on simultaneous antisolvent-vapour-induced precipitation and convective drying of a solute-containing droplet was extensively conducted since this technique was introduced. However, the internal droplet compositions, which were suggested to be related to the formation of particle morphologies, had not been explored. Herein, the ethanol-vapour-induced precipitation of multi-solvent droplets containing maltodextrin as the solute was used to analyse internal droplet compositions. The droplet mass and diameter profiles were obtained via an established single-droplet drying experiment, which mimicked the spray drying of droplets. Analysis revealed that the antisolvent concentration increased with time and was higher than solvent concentration towards the end of the process. It is interesting to find out that the final particle morphology was profoundly impacted by the ambient ethanol humidity and also how spontaneous the subsequent drying was during ethanol-vapour-induced precipitation of the solutes. The formation of the porous structure was favoured with the occurrence of spontaneous vaporization once the ethanol was present for precipitation. Therefore, low ethanol humidity (20% ERH in this study) was sufficient. In contrast, higher ethanol humidity (>70% ERH) was preferable to produce spherical particles. This study provides an insight into particle engineering to unveil the internal droplet conditions and physical phenomena during this unique process.

1. Introduction

Particle size reduction techniques have been advanced and implemented in various industries, such as the pharmaceutical sector, dairy and food manufacturing, to produce fine particles with enhanced functional and physico-chemical characteristics. For example, in the pharmaceutical field, a smaller particle size will promote effective drug delivery and higher bioavailability. In the food industry, a smaller powder size provides a larger surface area for water absorption, leading to a high dissolution rate which gives a better mouthfeel and flavour release. The techniques for producing fine powder in food [1] and pharmaceutical [2] industries have been critically reviewed. Typically in spray drying, this process involves the atomization of liquid feed to promote subsequent rapid solvent vaporization of the atomized droplets in the presence of a convective drying medium. The final size distribution of dried particles is typically in a range of tens to hundreds of microns, mainly controlled by the initial size of atomized droplets. In general, the overall particle size may be further reduced by atomizing the liquid feed to a sufficiently smaller droplet size. However, such a very fine droplet atomization would compromise the process throughput as the flow rates would be limited for routine production. From the commercial perspective, there is a demand for spraying the liquid droplets at high flow rates while producing large quantities of ultrafine particles, and ideally to be completed in a single step.

To address these issues, an innovative technique based on spray drying incorporated with antisolvent-vapour precipitation (AVP) was recently developed by a research team from Monash University. In this process, vaporized ethanol (in some cases, water vapour, depending on the nature of the solute) is mainly used as the antisolvent vapour and carried by inert nitrogen gas to form

Abbreviations: DE, Dextrose equivalent; EAH, Ethanol absolute humidity (kg/kg db); ERH, Ethanol relative humidity (%).

* Corresponding author.
E-mail address: wai.woo@auckland.ac.nz (M.W. Woo).

https://doi.org/10.1016/j.apt.2022.103440

a convective drying medium. The underlying principle of this technique is the absorption of antisolvent vapour into the solute-containing droplets to cause a gradual reduction in the solubility of dissolved particles, leading to precipitation. As a result, multiple micron-sized particles could be precipitated from a single droplet under atmospheric conditions [3]. Therefore, this technique could be a potential alternative to produce ultrafine powders in large amounts, which is remarkably different from the one-droplet-to-one-particle transition as observed in conventional spray drying.

The antisolvent-vapour precipitation approach was first reported using a sugar-based organic material, lactose [3]. Numerous lactose microspheres with diameters within the submicron range were precipitated from a single aqueous lactose droplet of an initial diameter of 1.2 mm. A series of experimental work was then undertaken to study the viability of antisolvent-vapour precipitation using different solute materials such as whey protein, maltose, maltodextrin, salt and composite particles [4–6]. Further qualitative studies on this innovative approach were conducted, including the effect of operating conditions on the morphologies of precipitated particle, as well as the mechanism of particle formation was proposed [7,8]. In the study of ethanol-vapour precipitation using the aqueous droplets of maltose or maltodextrin, it was interesting to observe a similar particle morphological transition: from porous, microsphere network and the discrete microspheres, with increasing ethanol humidity [4].

The precise particle morphology control by simply adjusting the ambient ethanol humidity still necessitates an exploratory investigation. Based on the experimental studies using aqueous droplets of lactose [7,8] and maltodextrin [4], the use of higher ethanol humidity of the drying stream was observed to favour the formation of the microspheres upon drying. It was qualitatively described by Tan *et al.* [4] that at a certain point of ethanol concentration within the droplet, the spherical particles were obtained upon drying. Herein, the formation of particle morphology could be related to the absorption behaviour of ethanol vapour and the change of the internal droplet compositions. To the best of the authors' knowledge, a quantitative study on the variation of internal droplet compositions throughout the process has not been performed up to this date. Therefore, it is important to investigate the profiles of internal droplet compositions to explain the formation of various particle morphologies.

In the present study, maltodextrin was used as the solute, ethanol as the antisolvent and water as the solvent. The behaviour of the aqueous maltodextrin droplets exposed to the convective medium consisting of ethanol vapour was examined using a newly established experimental setup of a single-droplet drying (SDD) approach. The SDD approach is effective in monitoring the droplet-to-particle process with a wide range of controlled operating conditions, mimicking to any possible extent of the spray dryer environment. In addition, integrated analyses on the drying kinetics and the evolution of droplet geometry can be carried out. Based on experimental results, i.e. the profiles of droplet mass and diameter, post analyses on temporal variations of component mass fractions of the droplet were then performed. The purpose is to further elucidate the formation of various particle morphologies by monitoring the change in the internal droplet compositions throughout the entire process.

2. Materials and methodology

2.1. Preparation of samples

In this experiment, a corn-based maltodextrin DE 18 powder was purchased from Melbourne Food Ingredient Depot. Ultrapure water obtained from a Milli-Q purification system (Millipore, Australia) was used throughout the experiment. The aqueous solutions of initial concentrations 2.5 wt% and 5 wt% were freshly prepared on the day of experiment by dissolving the powder in water. In generating nitrogen-ethanol gas flow, absolute grade $\geq$ 99.8% liquid ethanol (Merck, Australia) was used and ventilation nitrogen was supplied from a purchased nitrogen gas cylinder.

2.2. Experimental procedure

The single droplet approach was used to investigate the drying behaviours and the transformation of the droplet-to-particle process. The details of the working principle and setup of the glass filament SDD experiment have been described [9]. To incorporate the antisolvent-vapour precipitation with the single droplet drying in this study, the experimental rig was built and optimized by connecting an advanced control-evaporation-mixing (CEM) fluid delivery system to generate a drying medium carrying unsaturated ethanol vapour in the adjustable temperature and relative humidity. The *in-situ* droplet mass measurement was enhanced using a five-decimal microbalance (Mettler Toledo MS105DU). The schematic diagram of the experimental setup is displayed in Fig. 1. Brief descriptions are provided here for the sake of completeness.

The confined droplet chamber (label H in Fig. 1) was first preheated by flowing through nitrogen gas until a steady temperature, of which approximately half an hour was taken. The purpose is to minimize any ambient moisture which affects the absorption-evaporation process. By adjusting the flow rates via the control-and-readout unit (label L), liquid ethanol from the feed tank (label B) was then mixed with a fixed 8 L/min nitrogen gas to generate a conditioned gas using the control-evaporation-mixing (CEM) unit (label E). The flow rates of liquid ethanol and nitrogen gas were measured by the flowmeters (labels C and D, respectively). Once the temperature of the droplet chamber was stable, the conditioned gas stream was switched to the bypass (using the valve; labelled as F in Fig. 1) when generating and transferring the aqueous maltodextrin droplet into the drying chamber. This is to eliminate any undesirable absorption or evaporation of the droplet before the measurement and monitoring started. Single aqueous maltodextrin droplet of initial volume 2.0 μL was generated using a 5 μL gas chromatograph microsyringe (SGE Analytical Science Pty. Ltd., Australia) with an accuracy of ± 0.1 μL. The droplet was then suspended onto the tip of a glass filament (label J) positioned in the chamber using a separate transferring glass filament. The conditioned gas was immediately switched back to the chamber as the single droplet was placed in a chamber. The mass measurement and video recording of the droplet were conducted simultaneously. A high-definition video camera was used with back illumination of natural white light to monitor the droplet drying behaviour. This purpose is to generate a clear contrast between the outer droplet boundary and the background, which would ease the image analysis from the video, as described in the following section.

2.2.1. Image analyses: Droplet drying kinetics and particle morphology

After each experiment, the precipitated product was immediately collected onto a carbon stub and was sputter-coated before being observed using scanning electron microscopy (Phenom SEM). Internal and outer structures of each sample were observed.

In the droplet diameter (size) analyses, the video was first converted into JPEG images at one frame per second before the images were processed using ImageJ (National Institute of Health, USA) freeware. Time 0 of each set was firstly identified and the process was illustrated by a sequence of images corresponding to the drying time. The droplet projected area on each image (i.e. each second) was measured, and its equivalent diameter was computed by assuming the perfect circle of the projected area. In order to

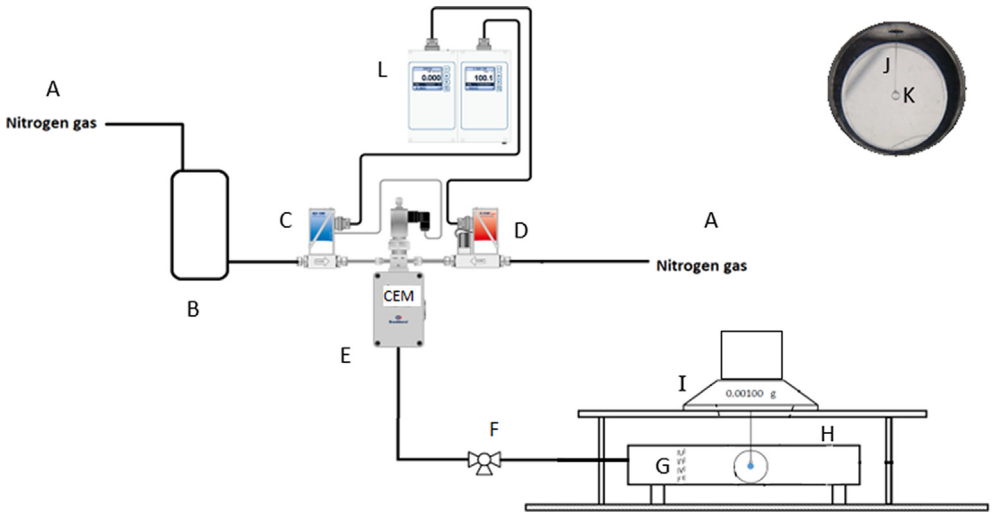

Fig. 1. Schematic diagram of experimental rig: A, nitrogen gas supply; B, liquid feed tank; C, liquid flowmeter; D, gas flowmeter; E, control-evaporation-mixing unit; F, bypass valve; G, stainless steel mesh layer; H, droplet chamber; I, microbalance; L, control-and-readout unit. Inset photograph: J, glass filament; K, sample droplet.

minimize the random error mainly caused at the beginning (time 0) of each experiment, the initial droplet volume was calculated from its known initial mass and density. The actual initial diameter was then calculated and used as a reference for calibrating the equivalent diameter of each image. The calibrated data were then used in the following calculations of droplet volume at each time. Droplet expansion or shrinkage (D/D_0) was also determined by normalizing the equivalent diameter at each time to the initial known droplet diameter at time 0.

The translucency of the droplet was analyzed using ImageJ freeware to detect the point where the droplet turns fully cloudy. The extracted images were first segmented and then converted to grayscale and binary form to obtain the distinct boundaries (droplet interface). Next, suitable values of brightness and contrast were set to improve the clarity between the droplet and its background to detect the transformation of the 'darkness' of the droplet (object of interest). The object which displays completely black indicates the droplet turns fully cloudy and opaque without any light reflection (see Figs. S1 and S2).

2.2.2. Experimental errors of droplet kinetics measurements

Generally speaking, the glass filament SDD approach possessed high reproducibility in measuring the droplet parameters, viz. mass and diameter [10]. The measurements were performed at least in duplicates and the results reported were the average data from at least two trials. Experimental errors between the repeated droplet mass measurements were within ±4–7% difference. Meanwhile, experimental uncertainty between the repeated diameter measurements at the initial stage was less than 5%. As the drying progressed, droplet diameter decreased until a kink was obtained, after which the rate of the decrease approached zero. The uncertainty became higher, approximately 8% towards the end of the drying process. The possible reason for the increased experimental uncertainty was that the precipitated particles were solidified to different shapes at the later stage, giving a large discrepancy between the resultant projected areas during diameter measurement.

2.3. Experimental conditions

The experiments were performed with a range of 0–95% ERH or 0–0.11 kg/kg db EAH under room temperature (22–25 °C). The temperature of the chamber was known by measurement using a thermocouple. The ethanol absolute humidity (EAH) was calculated from the known mass flowrates of liquid ethanol and nitrogen gas entering the CEM system. The ethanol relative humidity (ERH) of the gas stream at the operating (dry-bulb) temperature can be calculated using the following equations:

$$\textit{Ethanol relative humidity}\ (\%) = \frac{\textit{Partial vapour pressure of ethanol}}{\textit{Saturated vapour pressure of ethanol}} \times 100\% \tag{1}$$

$$\textit{Ethanol absolute humidity} = \frac{\textit{Liquid ethanol mass flowrate}(g/hr)}{\textit{Nitrogen mass flowrate}(g/hr)} \tag{2}$$

For simplicity, the ideal gas law equation was used to determine the ethanol partial vapour pressure at the operating temperature. The calculated EAH and ERH at the operating (dry-bulb) temperature were compared to the ethanol-nitrogen psychrometric chart [11], and insignificant disparity was found, indicating such estimations are valid. As a result, these parameters were easily controlled by adjusting the mass flow rate of liquid ethanol via the CEM system. Tables 1 and 2 list the process conditions used for aqueous droplets with initial concentrations of 2.5 wt% and 5 wt% maltodextrin DE 18, respectively. Note that 0% ERH acted as a control experiment with the use of nitrogen gas only as the drying medium, which can be considered similar to the drying air due to the fact that air consists of a high proportion of nitrogen.

3. Results

3.1. Droplet geometry evolution

The typical drying progress of a droplet exposed to the ethanol vapour laden nitrogen is depicted in Figs. 2 and 3. Under sufficiently high ethanol humidity, the droplet experienced uniform volume expansion accompanied by shrinkage throughout the process. It was noticed that the droplet lost its uniform shrinkage at some point towards the end of the process. The wrinkles with an irregular shape were then developed until a final shrivelled particle was obtained with no further change in mass.

Table 1
Experimental conditions, recorded maximum size, mass peak and relevant data for ethanol-vapour-precipitation and drying of 2.0 μL aqueous droplets with initial concentration of 2.5 wt% maltodextrin DE 18.

EAH (kg/kg db)	ERH (%)	Maximum mass, $m_{d,max}$ (mg)	Time of $m_{d,max}$ (sec)	Maximum ethanol mass fractions (at $m_{d,max}$)	D_{max}/D_0	Time of D_{max} (sec)	Time where fully cloudiness observed, t_{fc} (sec)	Ethanol mass fraction at t_{fc}	Morphology of precipitated particles	Average increment rate of ethanol mass fraction (sec^{-1})
0	0	–	–	–	–	–	–	–	Solid chunk	–
0.025	20	–	–	–	–	–	–	–	Porous	0.0035
0.054	50	2.14	60	0.095	1.02	60	220	0.493	Microsphere network	0.0016
0.066	60	2.18	190	0.236	1.08	330	200	0.305	Microsphere network	0.0019
0.074	70	2.52	220	0.354	1.12	320	140	0.163	Microsphere network	0.0023
0.088	75	2.58	250	0.750	1.17	290	120	0.473	Spherical	0.0030
0.100	80	2.74	245	0.759	1.18	320	120	0.419	Spherical	0.0033
0.102	95	3.05	320	0.954	1.23	365	115	0.417	Spherical	0.0045

Table 2
Experimental conditions, recorded maximum size, mass peak and relevant data for ethanol-vapour-precipitation and drying of 2.0 μL aqueous droplets with initial concentration of 5 wt% maltodextrin DE 18.

EAH (kg/kg db)	ERH (%)	Maximum mass, $m_{d,max}$ (mg)	Time of $m_{d,max}$ (sec)	Maximum ethanol mass fractions (at $m_{d,max}$)	D_{max}/D_0	Time of D_{max} (sec)	Time where fully cloudiness observed, t_{fc} (sec)	Ethanol mass fraction at t_{fc}	Morphology of precipitated particles	Average increment rate of ethanol mass fraction (sec^{-1})
0	0	–	–	–	–	–	–	–	Solid chunk	–
0.022	20	–	–	–	–	–	–	–	Porous	0.0023
0.074	65	2.37	200	0.182	1.08	265	150	0.128	Microsphere network	0.0020
0.084	70	2.48	280	0.816	1.14	295	140	0.498	Microsphere network	0.0021
0.090	80	2.78	270	0.812	1.19	335	130	0.394	Spherical	0.0019
0.100	89	2.98	285	0.887	1.22	325	120	0.373	Spherical	0.0031
0.110	95	3.21	310	0.946	1.26	295	105	0.381	Spherical	0.0038

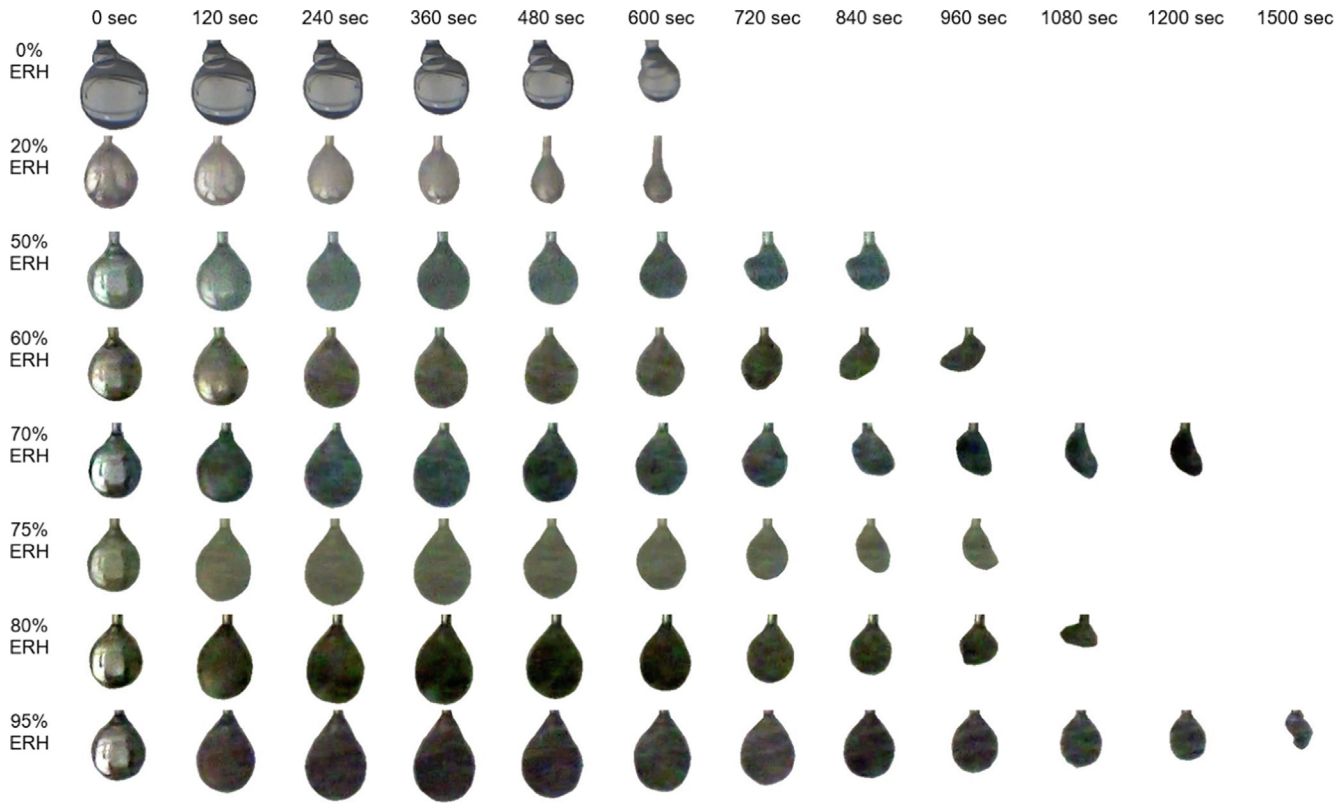

Fig. 2. Evolution of (initial concentration 2.5 wt%) maltodextrin droplet exposed to nitrogen gas and ethanol vapour.

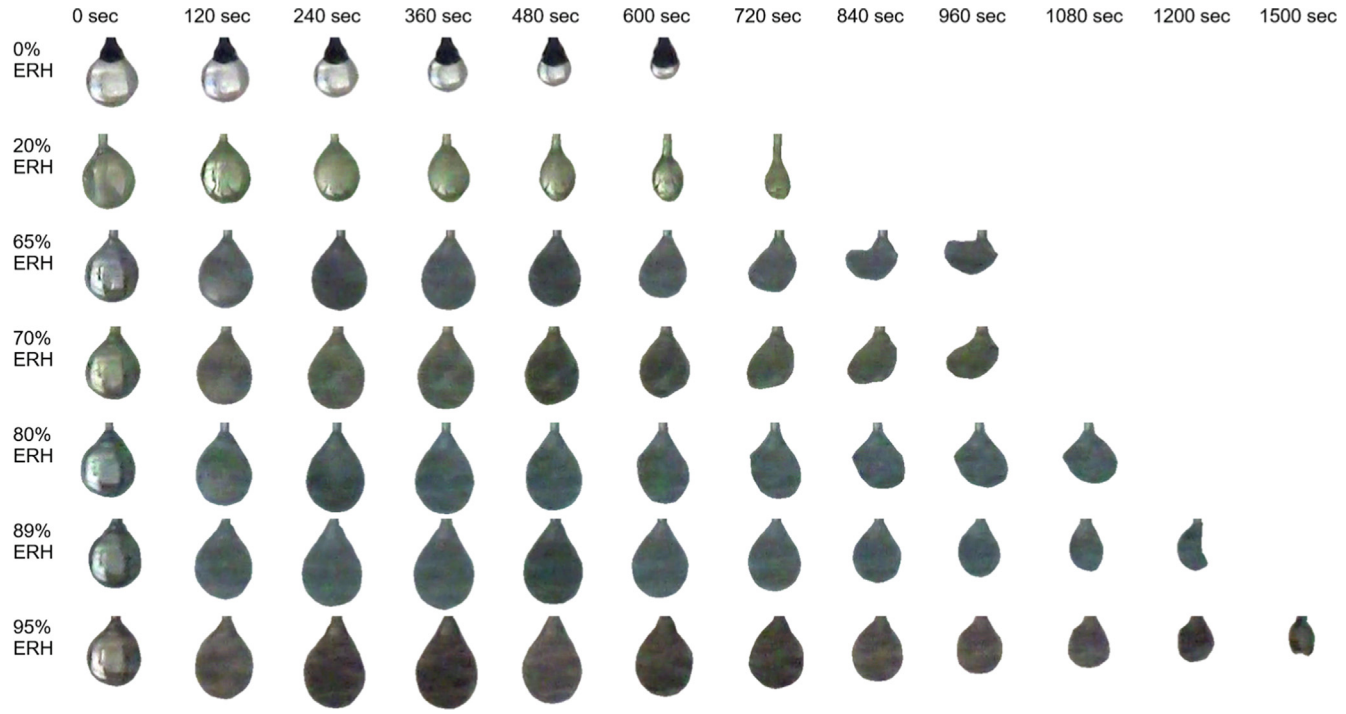

Fig. 3. Evolution of (initial concentration 5 wt%) maltodextrin droplet exposed to nitrogen gas and ethanol vapour.

3.1.1. Cloudiness analyses

A transparent droplet gradually turned turbid and eventually opaque throughout the process by visual observation. In view of the fact that maltodextrin is readily soluble in water and insoluble in ethanol, the presence of ethanol would result in the decrease of maltodextrin solubility in water, producing the precipitates from its dissolved state. Such phase transition could be evident by the development of cloudiness during the initial droplet expansion period, although the exact commencement was difficult to pinpoint. The binary images of the object progressively became entirely black (denoting the droplet turned completely cloudy) are shown in Figs. S1 and S2. Exceptional cases are 0% and 20% ERH conditions, where the droplet did not turn cloudy thoroughly even at the end of drying. For the control experiment 0% ERH, the droplet was experiencing purely water removal resulting in solidification during the drying process. For the 20% ERH case, the outcome suggests that insufficient ethanol was present in the droplet to reduce the solubility of the dissolved maltodextrin in the water phase. For the remaining conditions, the total time taken where the droplet turns completely cloudy since the commencement of the experiment is listed in Tables 1 and 2. As expected, a shorter time was required for the droplet to turn fully cloudy with increasing ambient ethanol humidity.

3.1.2. Morphologies of the final precipitated particles

A variety of particle morphologies obtained from this experiment are presented in Fig. 4, namely solid chunks (0% ERH), porous matrix (20% ERH), network of microspheres (50–70% ERH) and discrete microspheres (>75% ERH). It was found that the morphologies of maltodextrin particles formed are strongly affected by the ambient ethanol humidity, while the influence of initial solute concentration was not apparent. This observation was in line as reported by Tan *et al.* [4]. In their studies using the same initial solute concentrations of 2.5 wt% and 5 wt%, a transition from a network of microspheres to discrete microspheres was observed when ERH varied from 70% (or 65%) to approximately 95%. In the microsphere network, the microspheres were seemed to be entrapped in a solid matrix and agglomerated by the solid bridges, which is distinguishable from the formation of discrete microspheres. In our experimental studies, a transition from a network to discrete microspheres was also noticed under similar ERH ranges used by Tan *et al.* [4], regardless of the initial solute concentration. In particular, the transitional porous network morphology, much like Swiss cheese, was observed from the 20% ERH condition (where the droplet lifetime at 20% ERH was comparable to 0% ERH). The formation of pores within the particles had been confirmed due to the dehydration of the ethanol-rich region, which was produced from mixing aqueous maltodextrin with ethanol [12].

Based on the observations in this study and as reported by Tan *et al.* [4], the morphologies of the final particles produced are strongly influenced by the ambient ethanol humidity. For instance, a sufficiently high ethanol humidity would likely lead to the production of maltodextrin microspheres [4]. The question is how the internal composition (ethanol and water concentration) corresponds to these external conditions. Further analysis was undertaken in Section 3.3 to further understand the observed morphological changes.

3.2. Ethanol-vapour-precipitation and drying behaviour of aqueous maltodextrin droplets

Owing to the capability of the new setup to measure and record the real-time droplet mass during the experiment, the droplet mass histories during the ethanol-vapour-precipitation and drying process were able to be monitored directly (displayed in Fig. 5 with uncertainty within ±4–7% difference between the repeated data) at an interval of 5 s. A brief description of mass curves is as follows: for cases with sufficiently high ambient ethanol vapour, an initial stage of net mass gain was observed due to the predominant absorption rate of ethanol being higher than the removal rate of water. Such phenomena are more pronounced, particularly at 95% ERH, the highest ERH used in this study. Note that the droplet undergoes simultaneous water loss and ethanol absorption at its surface. Water evaporation throughout the process is expected

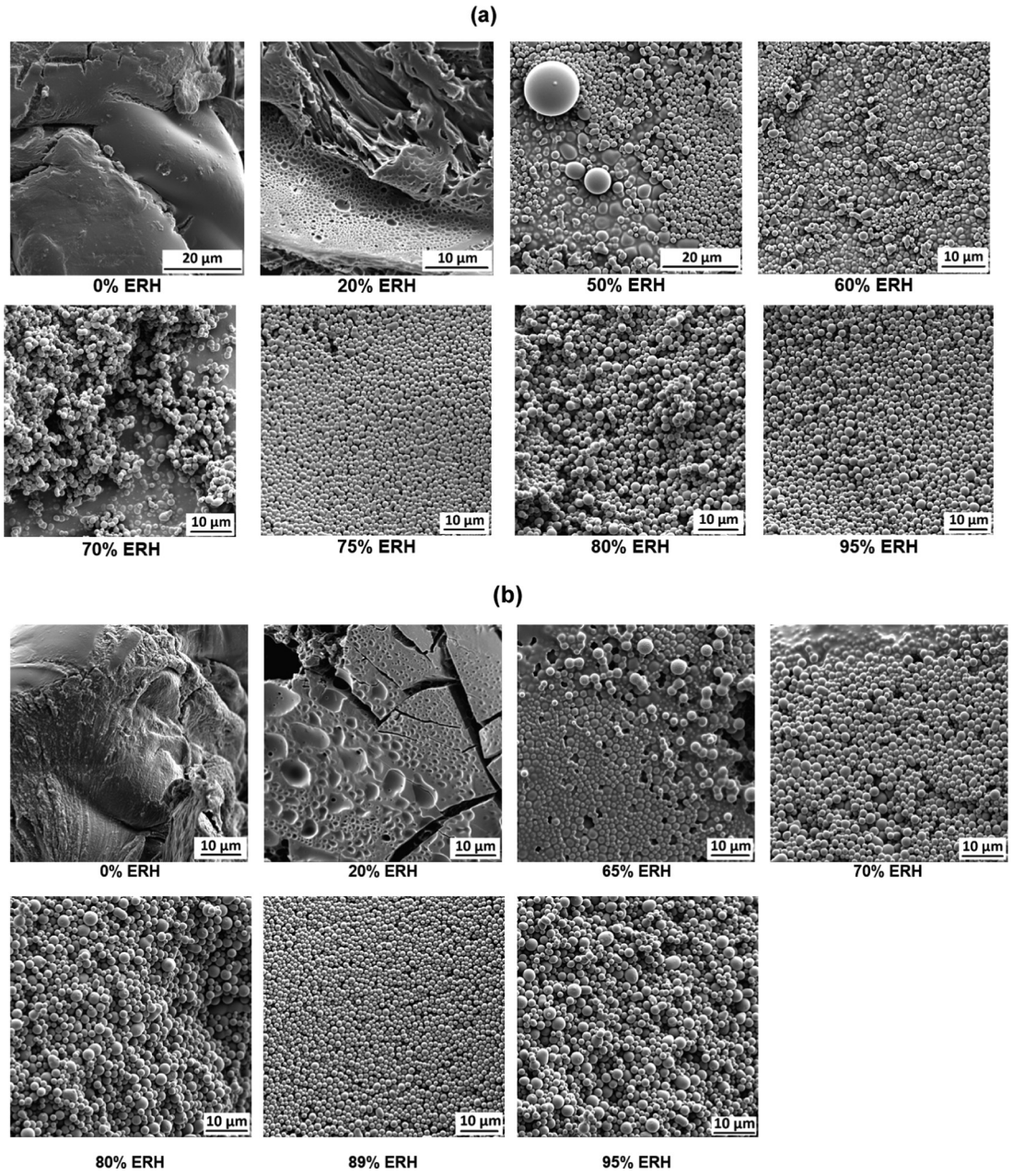

Fig. 4. The morphologies of maltodextrin particles after ethanol-vapour-induced precipitation and drying of droplets with initial solute concentrations of (a) 2.5 wt% and (b) 5.0 wt%

due to zero relative humidity of water vapour in the ethanol-nitrogen surrounding. Subsequently, net mass loss of the droplet was then observed as a result of continuous water removal with ethanol evaporation.

From the droplet mass profiles, the maximum droplet masses were obtained towards the end period of droplet expansion (except 0% and 20% ERH, where no mass peak was found). As expected, the values of maximum droplet mass and maximum diameter were getting larger with increasing ambient ethanol humidity. Such phenomenon is apparent for condition 95% ERH where the mass peak was the highest, i.e. 3.05 mg (additional $\sim$ 50%) and 3.21 mg (additional $\sim$ 60% mass increment from initial mass approximately 2.0 mg) for initial solute concentrations 2.5 wt% and 5.0 wt% respectively, comparing to the other conditions (<95% ERH). Moreover, since the start of the experiment, the corresponding time taken for a droplet to reach its maximum mass was longer with increasing relative humidity of ethanol. This could be explained by the larger ethanol concentration gradient existing between the droplet surface and its surrounding (at higher ambient ethanol humidity), such that the droplet could absorb a greater ethanol amount until a certain point before the net mass loss began to occur. In fact, the overall droplet lifetime at 95% ERH is also the longest (refer to Fig. 5) as the additional time required for drying off the precipitated particles.

Interestingly, a linear trend of mass decrease was observed after the mass peak when the net mass loss commenced until an abrupt kink was observed at the end of the process. The final masses were proportional to the mass of dissolved maltodextrin. Such linear trend has differed from the typical drying curve of droplets containing solutes (i.e. via hot drying air), where a progressive reduction in gradient was usually found, indicating the decreasing evaporation rates with time. In literature, this had been termed

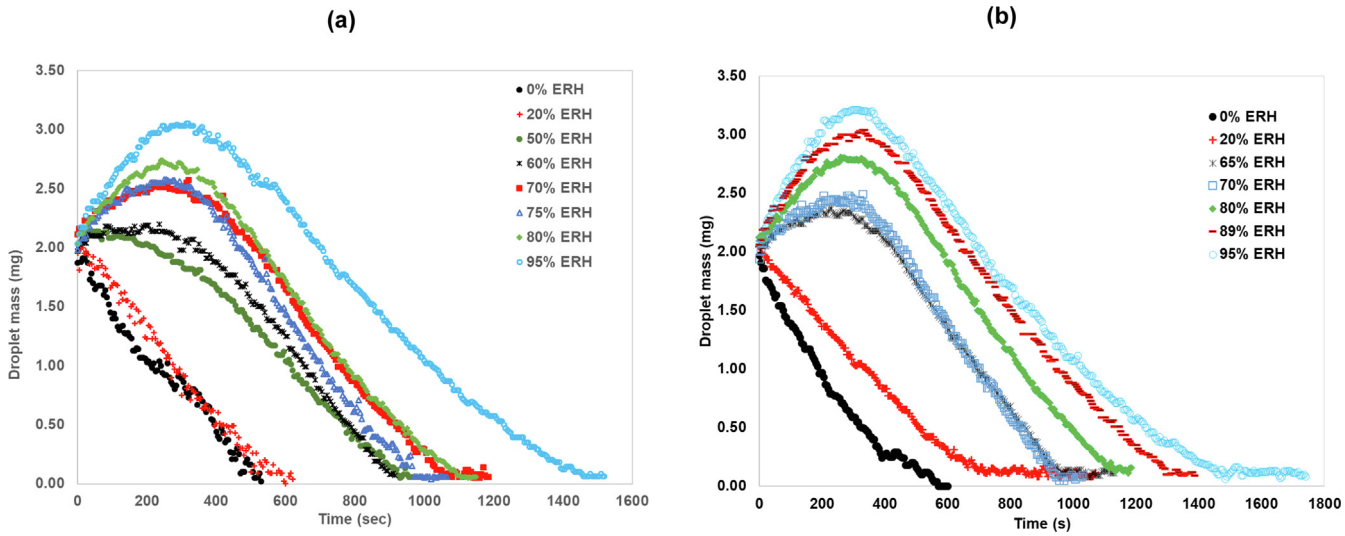

Fig. 5. Temporal mass profiles of aqueous droplet with initial maltodextrin concentrations of (a) 2.5 wt% and (b) 5.0 wt% corresponding to the conditions listed in Tables 1 and 2, respectively.

as falling rate behaviour. This is mainly due to the formation of solid crust at the droplet surface, which inhibits the moisture movement across the droplet surface. In our drying approach, it has been envisaged that a liquid suspension with uniform distribution of particles was formed [3]. Further discussion was undertaken in Section 4.3 to explain this observation in great detail.

The changing trend of normalized diameters, as shown in Fig. 6, is similar to the mass curve, consisting of an initial increment (indicating the droplet expansion) and a subsequent linear decline until a kink was reached at the final normalized diameters. These final values were attributed to the size of residual solid after drying. It is expected that the final normalized diameters with an initial solute concentration of 5 wt% should be larger than that of 2.5 wt%. The final normalized diameters were relatively consistent for the initial solute concentration of 2.5 wt% (approximately 0.55–0.65 on average). However, a board range (0.50–0.92 on average) was determined for 5 wt%, suggesting that the inevitable randomness of dried particles was formed in irregular shape, inducing significant error in predicting the internal compositions as described in the later sections. If we look closer at the cases of 89% and 95% ERH (giving the production of discrete microspheres), the final normalized diameter was lower (0.5–0.6), indicating that the mass loss was more efficient. This could be understood as such morphology allows the transport of liquid than retained in the particles due to lesser internal resistance between the microspheres formed under such conditions.

3.3. The changes in the droplet composition along the absorption-drying time

In this study, the data acquisition of droplet compositions via experimental methods is challenging, mainly due to the rapid drying of tiny droplets. In order to shed light on the changing trend of the internal droplet compositions, a simplified calculation was implemented to estimate the component mass fractions from the effective density of the droplets. The droplet density (ρ_{drop}) at each time was approximated using the measured droplet mass and volume (based on the equivalent diameter). The following

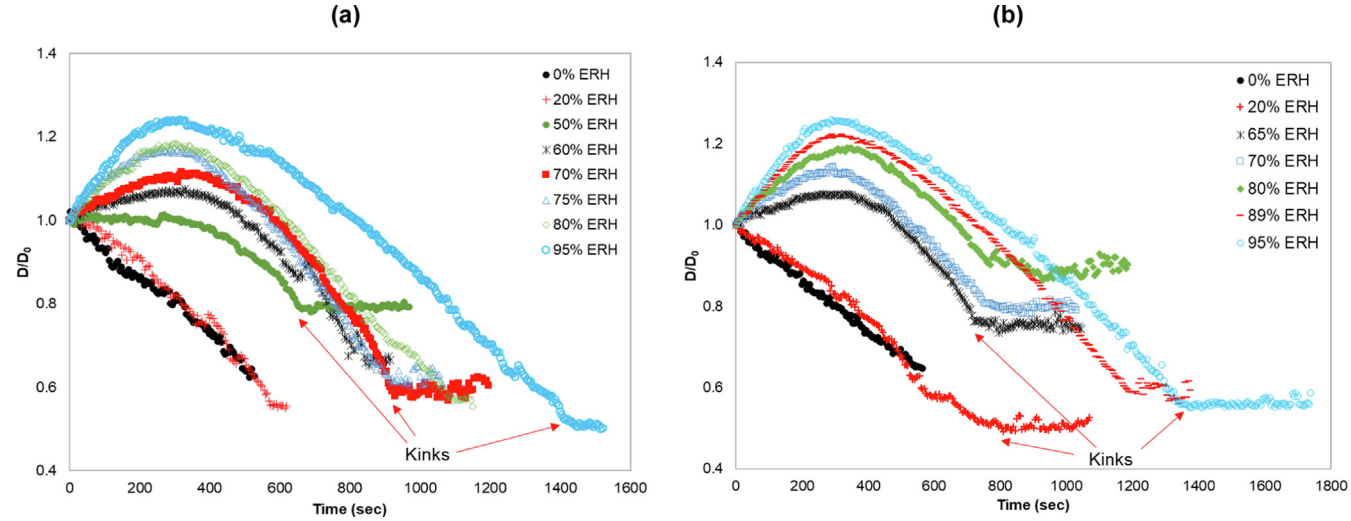

Fig. 6. Temporal shrinkage profiles of aqueous droplet with initial maltodextrin concentrations of (a) 2.5 wt% and (b) 5.0 wt% corresponding to the conditions listed in Tables 1 and 2, respectively.

relationships were used to predict the mass fractions of ethanol (x_E) and water (x_w), assuming ideal mixing:

$$\rho_{drop} = \frac{1}{\sum \frac{x_i}{\rho_i}} \tag{3a}$$

$$\frac{1}{\rho_{drop}} = \frac{x_E}{\rho_E} + \frac{x_w}{\rho_w} + \frac{x_m}{\rho_m} \tag{3b}$$

$$x_E + x_w + x_m = 1 \tag{4}$$

Eq. (3b) represents the mass-weighted density by factoring the densities of liquid components and pure maltodextrin (solute) with their respective mass fractions in the droplet. With the known parameters (droplet density (ρ_{drop}), pure-component densities (ρ_E, ρ_w and ρ_m) and mass of dissolved maltodextrin), mass fractions of ethanol (x_E) and water (x_w) can be estimated by substituting Eq. (4) into Eq. (3b), and upon rearrangement:

$$x_E = \frac{\frac{\rho_E \rho_w}{\rho_{drop}} - (1 - x_m)\rho_E - x_m \frac{\rho_E \rho_w}{\rho_m}}{\rho_w - \rho_E} \tag{5}$$

$$x_w = \frac{\frac{\rho_E \rho_w}{\rho_{drop}} - (1 - x_m)\rho_w - x_m \frac{\rho_E \rho_w}{\rho_m}}{\rho_E - \rho_w} \tag{6}$$

The whole evolutions of the predicted droplet density against time under various conditions are illustrated in Fig. S4 for initial maltodextrin concentrations 2.5 wt% and 5 wt%, respectively. A general description of the trend observed from these figures is provided as follows: Under the experimental condition, the initial droplet density (at time 0) was ~ 1000 kg/m^3, which is approximately equal to the pure water density (although the presence of a low amount of dissolved maltodextrin). It progressively reduced until a stage where plateau was observed and the duration was comparably longer. The droplet density was in the range of 750–800 kg/m^3 before an abrupt density decrease was noticed towards the end of drying. Note that the range of liquid ethanol density is 750–800 kg/m^3 under the experimental conditions. This suggests that the droplet consists of a relatively high quantity of ethanol than water during this period. The range of predicted densities from time 0 up to the plateau stage, which is between the densities of pure ethanol and pure water, is reasonable.

Beyond the plateau, a sudden drop (or increase in some cases, e.g. curve with 70% ERH in Fig. S4(a)) in the estimated droplet density was observed, corresponding to the moment when the kink was observed in Fig. 6. In fact, the density of precipitated particles at the end of the process does not equal to the real density of dry maltodextrin DE18 powder, which is 1330 ± 10 kg/m^3 [13]. This is because the droplet could not shrink further towards the end of the process, as shown in Fig. 6. The curves of diameter ratio reached a kink (labelled in Fig. 6), beyond where there is no further droplet size reduction. Meanwhile, the recorded droplet mass had shown a continuous decrease (until 2.5% or 5% of the respective initial mass). Therefore, the trend beyond the kink is not useful for the analysis of effective droplet density. The potential 'surface locking' was also noticed when approaching the kink. On this basis, the temporal evolutions of the predicted droplet density had been displayed (Fig. 7) up to approximately 200 s before the kink observed in the corresponding Fig. 6. In the following paragraph, the corresponding temporal profiles of droplet compositions were presented and discussed.

The predicted profiles of ethanol (antisolvent) and water (solvent) mass fractions within the droplet under various conditions are presented in Figs. 8 and 9 for initial solute concentrations of 2.5 wt% and 5 wt%, respectively. Typically, the water mass fractions had decreased from the initial values (approximately 97.5 wt% and 95 wt%, respectively) while ethanol mass fractions had linearly increased. This implies the absorption of ethanol and water vaporization across the droplet boundary as expected. As the drying progressed, ethanol concentration was maintained to be higher than water concentration in most cases.

In spite of a certain degree of uncertainty in estimating the component mass fractions in the droplet, the average increment rate of ethanol mass fraction ($\bar{x_E}$) was evaluated from the linear parts in Fig. 8 and Fig. 9, i.e. from the beginning to the stage where no drastic change in final ethanol mass fractions. It was expected that the value of $\bar{x_E}$ became greater with increasing ethanol humidity, indicating that a larger concentration gradient promotes the higher intake rates of ethanol into the droplet. From both experiment sets, however, the average increment rate $\bar{x_E}$ at 20% ERH was unusually higher than $\bar{x_E}$ at the condition of much higher ERH (except 95% ERH) under the same operating temperature. This may seem to contradict the previous sentence, where the average ethanol concentration within the droplet increased drastically under such low driving force at low ERH conditions. This unusual observation will be elucidated in the next section of this manuscript.

4. Discussion

4.1. Unusual rapid increase in ethanol concentration at low 20% ERH ambient condition

The primary difference in droplet absorption-dying behaviour between 20% ERH and the other conditions is that the former experiences continuous droplet shrinkage, whereas the droplets initially expanded before shrinkage for the latter. We will theoretically assess if this could have an impact on this unusual behaviour. The rate of mass transfer, denoted by the ethanol absorption rate below as a case in point, can be correlated to the mass-transfer coefficient (h_m), surface area (A_{drop}) and the concentration difference between the interface ($\rho_{E,s}$) and the bulk drying medium ($\rho_{E,\infty}$), as represented in Equation (7). The Ranz-Marshall equation [14,15] was used to evaluate the mass-transfer coefficient (Eq. 8).

$$\frac{dm_E}{dt} = h_m A_{drop}(\rho_{E,s} - \rho_{E,\infty}) \tag{7}$$

$$h_m = \left[2.0 + 0.6 Re^{\frac{1}{2}} Sc^{\frac{1}{3}}\right] \frac{\mathfrak{D}_{mix,Film}}{d_{drop}} \tag{8a}$$

$$h_m = \left[2.0 + 0.6\left(\frac{\rho_{\infty,Film} d_{drop} U_{rel}}{\mu_{mix,Film}}\right)^{\frac{1}{2}} \left(\frac{\mu_{mix,Film}}{\rho_{\infty,Film}\mathfrak{D}_{mix,Film}}\right)^{\frac{1}{3}}\right] \frac{\mathfrak{D}_{mix,Film}}{d_{drop}} \tag{8b}$$

where $\rho_{\infty,Film}$, $\mu_{mix,Film}$ and $\mathfrak{D}_{mix,Film}$ are density, dynamic viscosity and binary diffusivity of vapours located at the droplet-ambience interface respectively, were evaluated at film temperature. U_{rel} is the relative velocity between the droplet and the drying stream. Taking $\rho_{\infty,Film} = 1.15 kg/m^3$, $\mu_{mix,Film} = 1.5 \times 10^{-5} Pa.s$, $\mathfrak{D}_{mix,Film} = 2 \times 10^{-5} m^2/s$ and $U_{rel} = 0.2 m/s$, a plot of $h_m A_{drop}$ versus droplet diameter ranged up to 1.5 mm (initial droplet volume 2.0 μL) are presented in Fig. S3.

Considering the scenario where the droplet was initially exposed to the ambience of ethanol vapour, the absorption rate of ethanol into the droplet (represented by $h_m A_{drop}$) is theoretically increasing with a larger droplet diameter, as illustrated in Fig. S3. Therefore, from this perspective, one would expect the droplet initially experienced a relatively lower rate of ethanol absorption and water evaporation. Both factors would have contributed to a relatively slower increase in the ethanol concentration of the 20% ERH

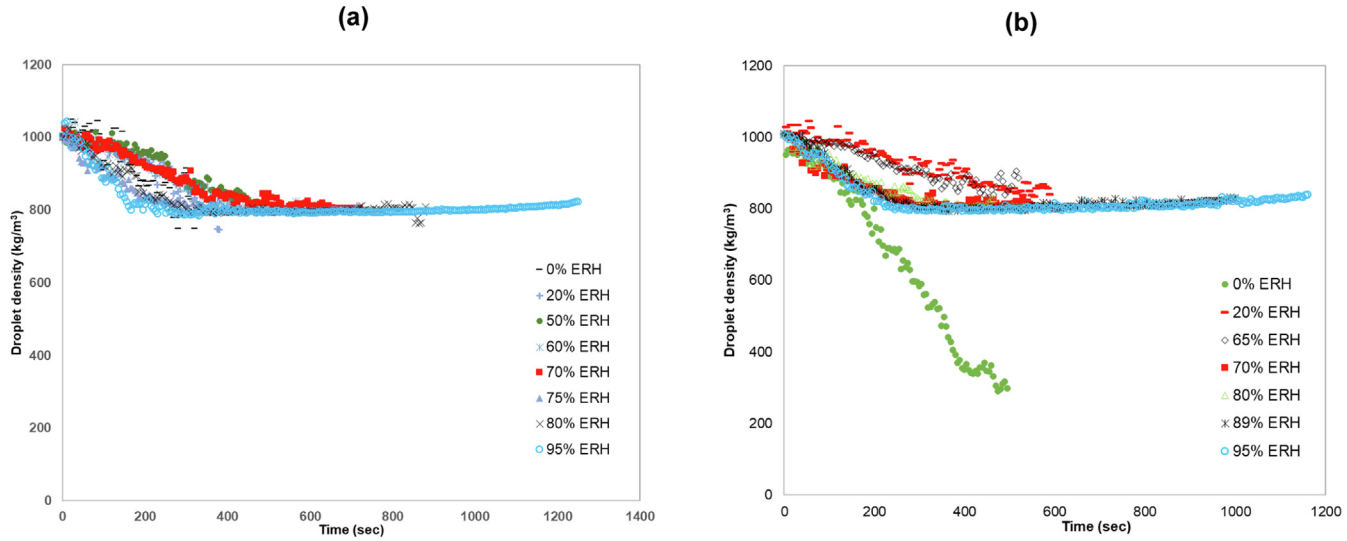

Fig. 7. Temporal overall density of aqueous droplet with initial maltodextrin concentrations of (a) 2.5 wt% and (b) 5.0 wt% corresponding to the conditions listed in Tables 1 and 2, respectively. Each curve ended at 200 s before the kink as in Fig. 6(a) and (b), respectively.

condition compared to other ethanol vapour ambient conditions in this study. Contributing to this factor, one would also expect higher ethanol humidity to produce a more rapid increment rate in the droplet ethanol concentration.

Unexpectedly, a comparably high increment rate of ethanol concentration within the droplet was found at ethanol humidity as low as 20%, relative to the 50–85% ERH condition. This suggests a phenomenon at the intermediate ethanol vapour condition that hinders either the ethanol absorption rate or the water evaporation rate. A recent analysis comparing a simultaneous droplet ethanol-water mass transfer model suggests the former [16]. One could imagine that the absorption flux was counteracted by evaporation flux across the droplet surface. This effect is apparent for intermediate high ERH range (e.g. 50–85% ERH), where the evaporation and absorption rates might be comparable. For low ethanol humidity (i.e. 20% ERH in this study), water evaporation from a droplet is the dominant process. Therefore, a high water removal rate would also lead to a high increment of ethanol concentration within the droplet. For extremely high ERH conditions (>90% ERH), the depression on the ethanol absorption rate may have been overcome by the high ethanol vapour concentration difference (driving force), leading to the highest increment rate of ethanol concentration compared to other conditions.

On this basis, the intermediate high ERH range may not yield a rapid increment rate of ethanol concentration within the droplet as performed as the low ERH condition. The porous structure would be favourably obtained under the conditions of low ethanol humidity with subsequent dehydration. In the following part, the internal condition of the droplet, which leads to different particle morphologies (i.e. porous and microspheres), will be discussed in more detail.

4.2. Effect of spontaneous quenching during ethanol-vapour-induced precipitation on the morphology formation

The particle morphology produced under 20% ERH condition in this study may beckon the following question: why was the porous structure formed instead of the expected microspheres, despite the high ethanol concentration of droplet above 90 wt% obtained? According to the proposed mechanism by Tan *et al.* [4], the absorption and concentration of ethanol in the droplet were limited at low ERH, resulting in the formation of porous structure upon drying. In contrast, the spherical particles were produced when a sufficiently high amount of ethanol was absorbed by the droplet. However, this statement contradicts the 20% ERH in our study that the average increment rate $\bar{x}_E$ was not limited but unusually higher than other conditions. As discussed in Section 4.1, such a rapid increment rate in ethanol concentration (due to rapid ethanol absorption rate) may not be the determining factor for the demarcation between the formation of porous structure and the microspheres.

Another crucial factor in answering such morphology formation might be related to the following question: how does the solute concentration within the droplet change during the simultaneous ethanol absorption and dehydration process? To examine the variation of solute mass with respect to the liquid mass throughout the process, two parameters, namely the mass ratio of solute-to-liquid and mass ratio of ethanol-to-water, were evaluated to compare the compositions within a droplet. Note that the solute is maltodextrin, while the liquid mass is the total mass of ethanol plus water. The plots of mass ratio of solute-to-liquid against the mass ratio of ethanol-to-water are illustrated in Figs. S5 and S6. Fig. 10 displays the enlarged portion of Figs. S5 and S6, up to the point where the respective maximum droplet masses were achieved. All plots begin from approximately 0.025 and 0.050 g of maltodextrin / g of liquid, respectively. In view that the mass of solute was fixed, an increase in mass ratio of solute-to-liquid indicates a net mass loss of a droplet, and vice versa. The mass ratio of ethanol-to-water was continually increasing, mainly due to continuous water removal from the droplet.

Based on the results, the mass ratio of solute-to-liquid escalated drastically within a short time frame at low ethanol vapour density in the drying medium (i.e. 20% ERH). Such trend was also observed for 50% ERH using an initial 2.5 wt% maltodextrin droplet, although the increasing gradient was comparably lower. This might justifiably imply that the droplets underwent spontaneous quenching during the antisolvent precipitation (in the presence of ethanol). For the other cases (>20% ERH), an initial decline in the mass ratio of solute-to-liquid was observed from Fig. 10, and no significant change afterwards. The mass ratio of solute-to-liquid was then increased after the maximum droplet mass (see Fig. S5 and Fig. S6 in Supplementary Material). This indicates that under these conditions, the droplets experienced an initial net mass gain resulting from a predominant ethanol absorption, accompanied by the

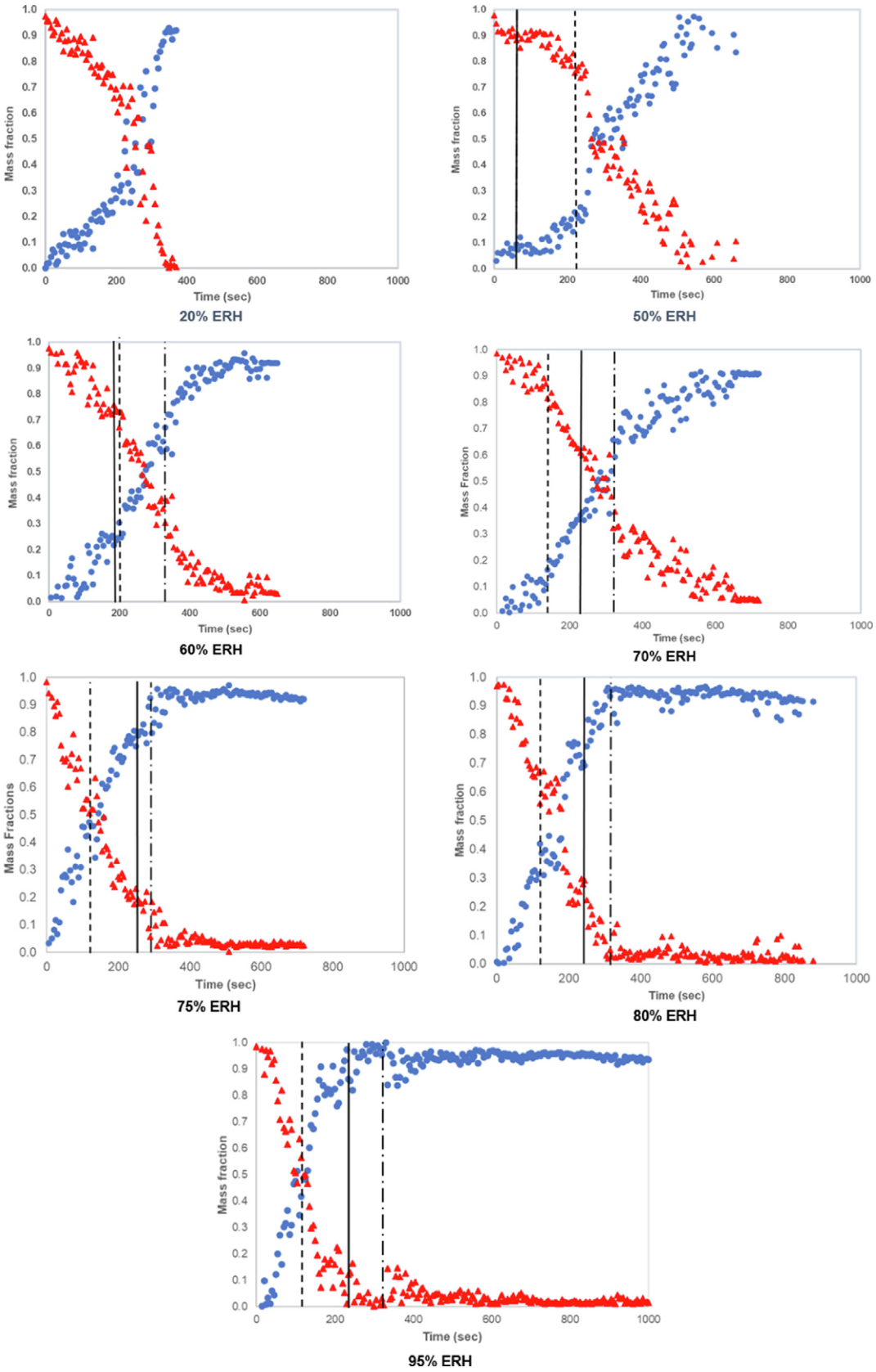

Fig. 8. Temporal mass fractions within aqueous droplet of initial maltodextrin concentration of 2.5 wt% during ethanol-vapour-induced precipitation and drying (Red triangles: water mass fraction; blue dots: ethanol mass fraction). For vertical lines, solid: mass peak; dash: full cloudy; dash-dot: maximum diameter recorded

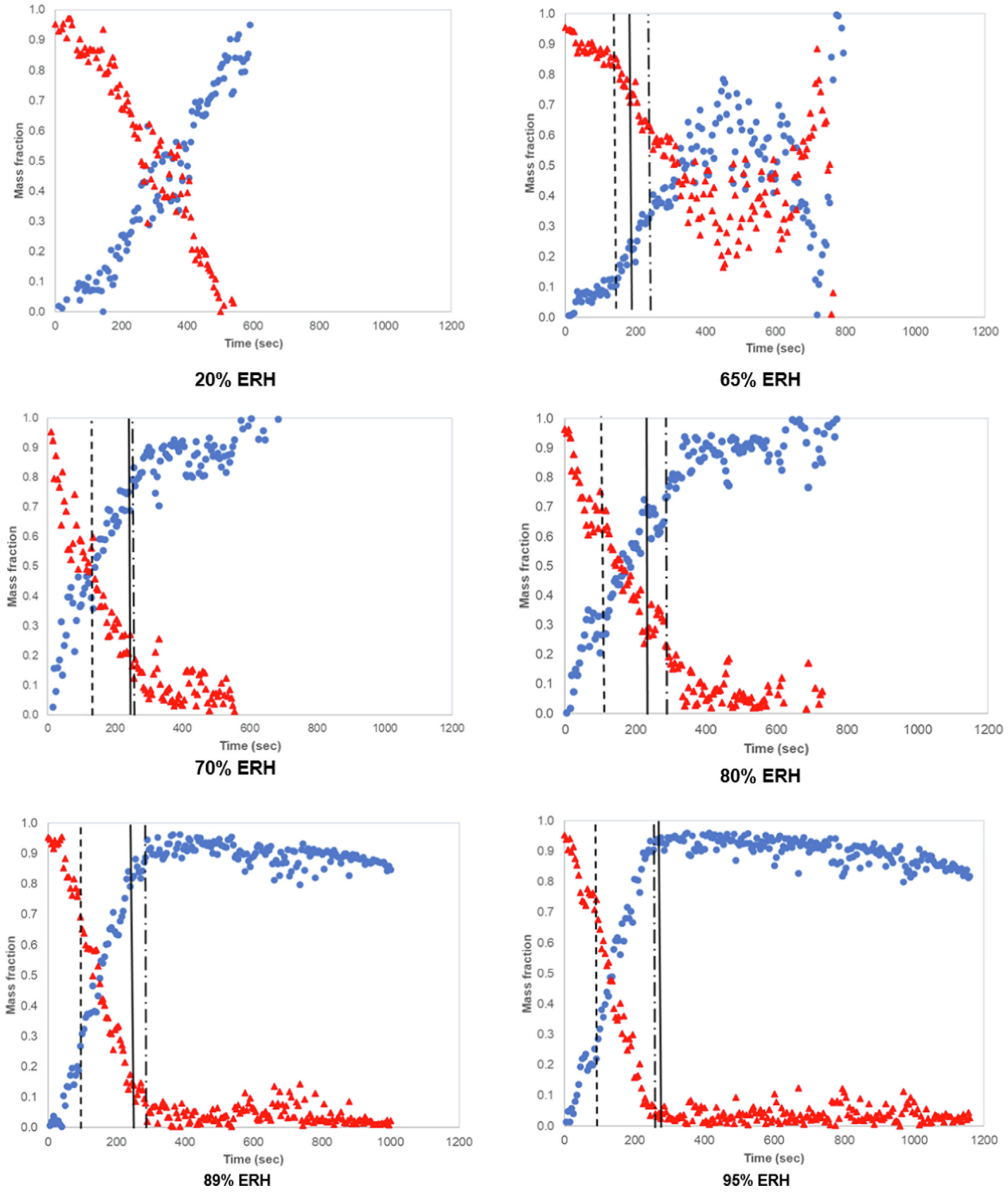

Fig. 9. Temporal mass fractions within aqueous droplet of initial maltodextrin concentration of 5.0 wt% during ethanol-vapour-induced precipitation and drying (Red triangles: water mass fraction; blue dots: ethanol mass fraction). For vertical lines, solid: mass peak; dash: full cloudy; dash-dot: maximum diameter recorded.

vaporization of both solvent and antisolvent in a much later time and the microspheres were obtained. This could be explained based on the proposed mechanism by Tan *et al.* [4]: At high ethanol humidity conditions, a larger driving force was created and a continuous net increase of ethanol within the droplet would result in the shrinkage of the water-maltodextrin phase and the coalescence of water-ethanol bubbles. As the rapid quenching did not occur spontaneously, further shrinkage would be proceeded, leading to the "pinch-off" mechanism [8] in producing the discrete spherical particles. At low ethanol humidity conditions, rapid quenching is

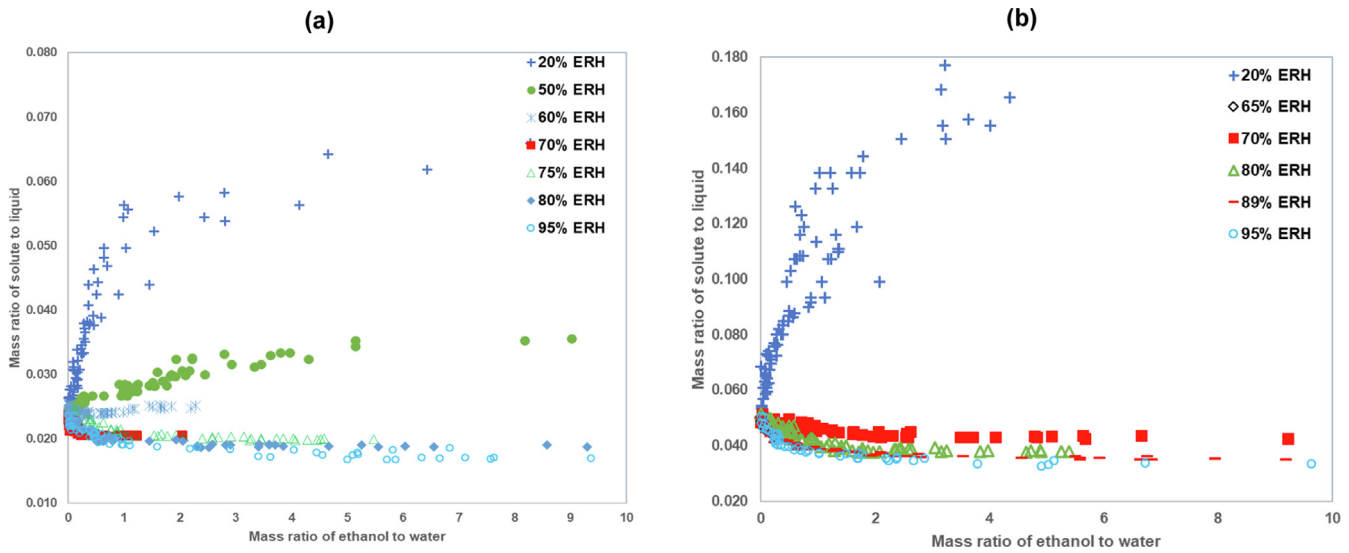

Fig. 10. Profiles of solute-to-liquid mass ratio against ethanol-to-water mass ratio within aqueous droplet of initial maltodextrin concentrations of (a) 2.5 wt% and (b) 5.0 wt% during ethanol-vapour-induced precipitation and drying. The curve ended at time when the respective maximum mass was recorded.

likely to occur, which might impede the further shrinkage of the water-maltodextrin phase and hence no discrete microsphere was produced. Therefore, such porous structure formation has usually pertained to the use of low ethanol humidity, which is sufficient for ethanol-vapour-induced precipitation.

In summary, the key factor in forming the porous structure is essentially the spontaneous quenching during the ethanol-vapour-induced precipitation. Several experiments have been performed to support this concept [4,12]. In their study, an initially aqueous maltodextrin droplet that just turned cloudy in the presence of ethanol (90% ERH was used by Tan *et al.* [4]) was removed for microscopic inspection. A liquid phase constituted of suspended bubbles was then observed. Subsequent dehydration gave a solid matrix with pores [12], similar to the porous particles obtained in our study.

Based on the aforementioned findings, we recommend that the formation of the porous structure is facilitated with spontaneous quenching once ethanol vapour was absorbed by the droplets for precipitation. Note that the specific ERH range might be dependent on other factors, such as process scale. In this study, a low ambient ethanol humidity (20% ERH) may be sufficient to precipitate the solutes, leading to a relatively short process time. From the perspective of industrial applications that may potentially utilize the ethanol-vapour-induced precipitation, we suggest that a strategy of using low ethanol humidity of the convective medium entering the spray chamber is sufficient for producing particles in the porous structure. In contrast, for the formation of spherical particles, high enough ethanol concentration within the droplet is essential to allow precipitation to occur before vaporization. Hence, the use of high ethanol humidity (>70% ERH in this study) is encouraged, and a relatively long process time might be observed. Consequently, discrete spherical particles can be acquired using the convective stream approaching 100% ERH, despite the requirement of high ethanol supply into the spray dryer.

4.3. Remarks on the drying behaviour of binary ethanol-water droplets with precipitated particles

In the experiment using high ethanol humidity, subsequent linear mass reduction after the mass peak experienced by the droplet could be explained as follow: As opposed to conventional convective droplet drying, the presence of the antisolvent (ethanol in this study) in the aqueous droplet might prevent the formation of solid crust at the droplet interface due to the insolubility of maltodextrin in ethanol. To be specific, the droplet interface had first to be exposed to high ethanol (antisolvent) vapour density in the drying medium throughout the entire process. During the process, the mass fraction of water was predicted to be less than ethanol throughout the net mass loss. As observed from Figs. 8 and 9, the mass fraction of ethanol was maintained to be higher than water after the mass peak. As a result, we propose that a relatively large-sized matrix of precipitate is unlikely to be formed due to the abundance of ethanol in the droplet. The size of precipitated maltodextrin would be as small as possible, forming the liquid suspension to provide easy removal of liquid (water and ethanol) prior to complete drying. From practical perspective, a uniform suspension with a high ethanol-to-water mass ratio in the droplet would potentially experience rapid dehydration. Thus, smaller size of the spray dryer chamber should be sufficient to obtain dried final products after antisolvent precipitation.

5. Conclusion

A thorough examination of the changing trend of internal droplet compositions was performed to understand better the formation of various particle morphologies from a single aqueous maltodextrin droplet exposed to a convective drying medium with varying ethanol humidity. The coupled analyses of drying kinetics (i.e. droplet diameter and mass) and the evolution of droplet geometry were facilitated via an established single-droplet drying experiment that mimicked the actual droplet drying process in a spray dryer. The depression on the absorption rate experienced by the droplets, along with the simultaneous evaporation, was noticed in this study. Apart from the ambient ethanol humidity, the final particle morphology was influenced by the spontaneous vaporization of the droplet during the precipitation in the presence of ethanol vapour. Low ethanol humidity is sufficient to promote ethanol-vapour-induced precipitation and spontaneous quenching to obtain porous particles. For the formation of microspheres, high ethanol humidity is desired for the precipitation and to prevent spontaneous quenching. Note that the specific ethanol humidity range depends on other factors, such as the process scale. The knowledge gained from this work can be used as a basis for a strategy to control the production of a specific particle morphology

with desired functionalities via simultaneous ethanol-vapour-induced precipitation and convective droplet drying.

Declaration of Competing Interest

The authors declare that they have no known competing financial interests or personal relationships that could have appeared to influence the work reported in this paper.

Acknowledgements

The authors would like to acknowledge the financial support provided by the ARC Research Hub for Computational Particle Technology (IH140100035) for the project. The first author would like to thank Monash University for the scholarship awarded (Monash Graduate Scholarship and Faculty of Engineering International Postgraduate Research Scholarship) to undertake the research.

Appendix A. Supplementary data

Supplementary data to this article can be found online at https://doi.org/10.1016/j.apt.2022.103440.

References

[1] T. Chen, M. Zhang, B. Bhandari, Z. Yang, Micronization and nanosizing of particles for an enhanced quality of food: A review, Crit. Rev. Food Sci. Nutr. 58 (6) (2018) 993–1001, 10.1080/10408398.2016.-1236238.
[2] R. Kumar, A.K. Thakur, P. Chaudhari, N. Banerjee, Particle Size Reduction Techniques of Pharmaceutical Compounds for the Enhancement of Their Dissolution Rate and Bioavailability, J. Pharm. Innov. (2021), https://doi.org/10.1007/s12247-020-09530-5.
[3] S. Mansouri, N. Fu, M. Woo, X. Chen, Uniform Amorphous Lactose Microspheres Formed in Simultaneous Convective and Dehydration Antisolvent Precipitation under Atmospheric Conditions, Langmuir 28 (39) (2012) 13772–13776, https://doi.org/10.1021/la302301h.
[4] J.Y. Tan, V.M. Tang, J. Nguyen, S. Chew, S. Mansouri, K. Hapgood, X.D. Chen, M. W. Woo, Unveiling the mechanism of antisolvent vapour precipitation in producing ultrafine spherical particles, Powder Technol. 275 (2015) 152–160, https://doi.org/10.1016/j.powtec.2015.01.059.
[5] S. Mansouri, X.D. Chen, M.W. Woo, Design of micron-sized salt particles by ethanol vapour drying, Powder Technol. 323 (2018) 558–562.
[6] S. Mansouri, M.W. Woo, X.D. Chen, Making Uniform Whey, Lactose, and Composite Lactose-Whey Particles from the Dehydration of Single Droplets with Antisolvent Vapor, Dry. Technol. 31 (13-14) (2013) 1570–1577, https://doi.org/10.1080/07373937.2013.807284.
[7] S. Chew, S. Mansouri, D. Wardhana, A. Mukhyiddin, N. Buchmann, K. Hapgood, X.D. Chen, M.W. Woo, Lactose microparticle formation from finely atomised droplets, Chem. Eng. Sci. 122 (2015) 395–402, https://doi.org/10.1016/j.ces.2014.10.001.
[8] S. Mansouri, G. Chin, T. Ching, M. Woo, N. Fu, X. Chen, Precipitating smooth amorphous or pollen structured lactose microparticles, Chem. Eng. J. 226 (2013) 312–318, https://doi.org/10.1016/j.cej.2013.04.051.
[9] S.X.Q. Lin, X.D. Chen, Improving the Glass-Filament Method for Accurate Measurement of Drying Kinetics of Liquid Droplets, Chem. Eng. Res. Des. 80 (4) (2002) 401–410, https://doi.org/10.1205/026387602317446443.
[10] N. Fu, M.W. Woo, X.D. Chen, Single Droplet Drying Technique to Study Drying Kinetics Measurement and Particle Functionality: A Review, Dry. Technol. 30 (15) (2012) 1771–1785, https://doi.org/10.1080/07373937.2012.708002.
[11] D.C. Shallcross, Preparation of psychrometric charts for alcohol vapours in nitrogen, Korean J. Chem. Eng. 17 (1) (2000) 93–100, https://doi.org/10.1007/BF02789260.
[12] P.L. Xiao, S. Mansouri, V. Suriya Hena, Y.K. Bong, K. Hapgood, M.W. Woo, Spontaneous ethanol–water emulsification as a precursor for porous particle formation: Understanding the role of dissolved carbohydrates, Particuology 44 (2019) 44–53, https://doi.org/10.1016/j.partic.2018.06.004.
[13] C.Y. Takeiti, T.G. Kieckbusch, F.P. Collares-Queiroz, Morphological and Physicochemical Characterization of Commercial Maltodextrins with Different Degrees of Dextrose-Equivalent, Int. J. Food Prop. 13 (2) (2010) 411–425, https://doi.org/10.1080/10942910802181024.
[14] W.E. Ranz, W.R. Marshall, Evaporation from drops: Part 1, Chem. Eng. Prog. 48 (3) (1952) 141–146.
[15] W.E. Ranz, W.R. Marshall, Evaporation from drops: Part 2, Chem. Eng. Prog. 48 (4) (1952) 173–180.
[16] K.S. Lim, B. Adhikari, J. Xiao, X.D. Chen, C. Selomulya, M.W. Woo, A reference-component coordinate system approach to model the mass transfer of a droplet with binary volatiles, Dry. Technol. (2021) 1–20, https://doi.org/10.1080/07373937.2021.2000431.